Biotechnology Reports 30 (2021) e00612

Contents lists available at ScienceDirect

Biotechnology Reports

journal homepage: www.elsevier.com/locate/btre

Biogenic nanosized gold particles: Physico-chemical characterization and its anticancer response against breast cancer

Neelu Singh[a,1], Monoj Kumar Das[b,1], Aftab Ansari[c], Dambarudhar Mohanta[c], Paulraj Rajamani[a,*]

[a] School of Environmental Sciences, Jawaharlal Nehru University, New Delhi, 10067, India
[b] Cancer Genetics and Chemoprevention Research Group, Department of Molecular Biology and Biotechnology, Tezpur University, Napaam, Tezpur, 784028, Assam, India
[c] Nanoscience and Soft Matter Laboratory, Department of Physics, Tezpur University, Napaam, Tezpur, 784028, Assam, India

ARTICLE INFO

Article history:
Received 28 September 2020
Received in revised form 17 January 2021
Accepted 23 March 2021

Keywords:
Biosynthesized
Gold nanoparticles
Anticancer
Antiproliferation

ABSTRACT

With the advancement of nanotechnology, the nano-sized particles make an imprint on our daily lives. The present investigation revealed that biomolecules present in seed exudates of Vigna radiata are responsible for the synthesis of AuNPs, confirmed by the routine characterization techniques. Anticancer efficacy showed by AuNPs might be due to the release of phytochemicals in the exudate which is being adsorbed on the surface of AuNPs referencing their anticancer efficacy against the tested breast cancer cell lines. Inhibition of clonogenicity and cell cycle arrest at G2/M phase then apoptosis of AuNPs was also observed, but found nontoxic to the human PBMC cells which further confirms its biocompatible property Among the various physicochemical study, present AuNPs shows unique information, they show photoluminescent property which may be used for bioimaging purposes. However, further molecular analysis needs to be explored to understand the underlying mechanism for therapeutic and biomedical application.

1. Introduction

Breast cancer is not only a highly complex and heterogeneous disease but also one of the common malignancies found among women, responsible for almost 30 % new cases every year [1,2]. In general five subtypes of breast cancer are identified, which are categorized through gene expression and by the immune-histochemical expression of various receptors *viz.* estrogen receptor [ERα], progesterone receptor [PR] and human growth receptor 2 [HER 2] [1]. Available modes of treatments such as surgery, hormonal, chemo, and radiation therapy are not well enough as they come up with certain limitations, among which most common is their non-specificity between normal and cancer cells, resulting in their inevitable side effects. This spark the scientist to continue up in the search of a certain drug, or mode of delivery of drugs which are cancer tissue-specific causing minimal side-effect on normal cells. In this purview, advancement in the field of nanotechnology showed an optimistic approach, as it operates at nano-level [specifically at 1–100 nm], with a range of physicochemical diversity, thus being employed in various areas but their biomedical applications are quite impressive, where they are being used for sensors, imaging, drug delivery [3]. In this line among various studied nanoparticles, Gold nanoparticles [AuNPs] have shown their impressive potential right from imaging to cancer therapy and drug delivery in both *in-vivo, in-vitro* systems [4] as revealed by literature survey. However, present synthetic routes of NPs involve methods like ion sputtering, hydrothermal, chemical reduction, and sol-gel processes but these techniques have proven to not only as expensive but also involve the usage of hazardous chemicals with minimal consideration for sustainability to both biological as well as on environmental basis. Therefore, increasing thrust has been given to those synthetic routes of nanoparticles which are not only cost-effective but also ecofriendly focusing the usage of bio-based products includes plant extracts, microbes, and enzymes [5,6], thereby eliminating many constraints like there availability and cost-effectiveness. And in support of the efficacious use of these biosynthesized nanoparticles number of published articles came up exhibiting their anticancer potential [3,7–9]. The phytochemical profile of *Vigna radiata* revealed that it is not only rich in various bioactive

* Corresponding author at: School of Environmental Sciences, Jawaharlal Nehru University, New Delhi, 10067, India.
E-mail address: paulrajr@yahoo.com (P. Rajamani).
[1] Authors equally contributed.

https://doi.org/10.1016/j.btre.2021.e00612

compound but also being used as antipyretic, antiscorbutic, against rheumatism and neuro-diseases in different parts of the world [10]. Therefore, the present study aims for the biogenic reduction of AuNPs using seed exudate of *Vigna radiata.* Thus, synthesized AuNPs will be characterized using sophisticated techniques such as EDX, XRD, SEM, HRTEM, and Photoluminescence, later assessed their anticancer potential [MTT and Alamar assay] against various exposed breast cancer cell lines MCF-7, MDA-MB-453, MDA-MB-435S, MDA-MB-231, MDA-MB-468. Further, the differential behavior of the AuNPs was scored on the normal cells [PBMC]. This opens up the scope of further investigations in the dimension of the synthetic application of biologically reduced gold nanoparticles and their potential application in treatment of cancer (Fig. 1).

2. Materials and methods

2.1. Materials

Mung (*Vigna radiata)* bean seed was obtained from local market, Tetrachloroauric acid [$HAuCl_4$], Dulbecco's Modified Eagle Medium [DMEM], Fetal Bovine Serum, Trypsin, purchased from Himedia, Dimethylsulphoxide [DMSO], Crystal violet, Trypan blue, Ethidium Bromide, Acridine orange, MTT, Alamar Blue, Phosphate buffered saline [PBS], Methanol etc ere obtained from Thermo scientific.

2.2. Synthesis of gold nanoparticles

The AuNPs were synthesized in a simple, one-step process described by Lukman et al. [37]. Briefly, seeds of *Vigna radiata* (Mung bean) purchased from the grocery store and was surface sterilized through 1% H_2O_2, followed by washing thrice and soaked in water 4 g/10 mL of distilled water and kept overnight in dark at normal room temperature. Next day, the residue was centrifuged at 6000 rpm for 5 min and filtered with whattman filter paper No.1. Filtrate was used as a bio-reductant. 10 mM gold solution was added, to the round bottom flask containing seed exudate while stirring, and left for 4–6 h. Thus, prepared AuNPs observed by the change in color centrifuged and washed twice and then lyophilized, collected dried sample was used for further study.

2.3. Characterization of biosynthesized AuNPs

Characterization of the surface morphology of AuNPs of the vacuum dried samples loaded on copper stub was examined under field emission scanning electron microscopy [FE-SEM Tescan

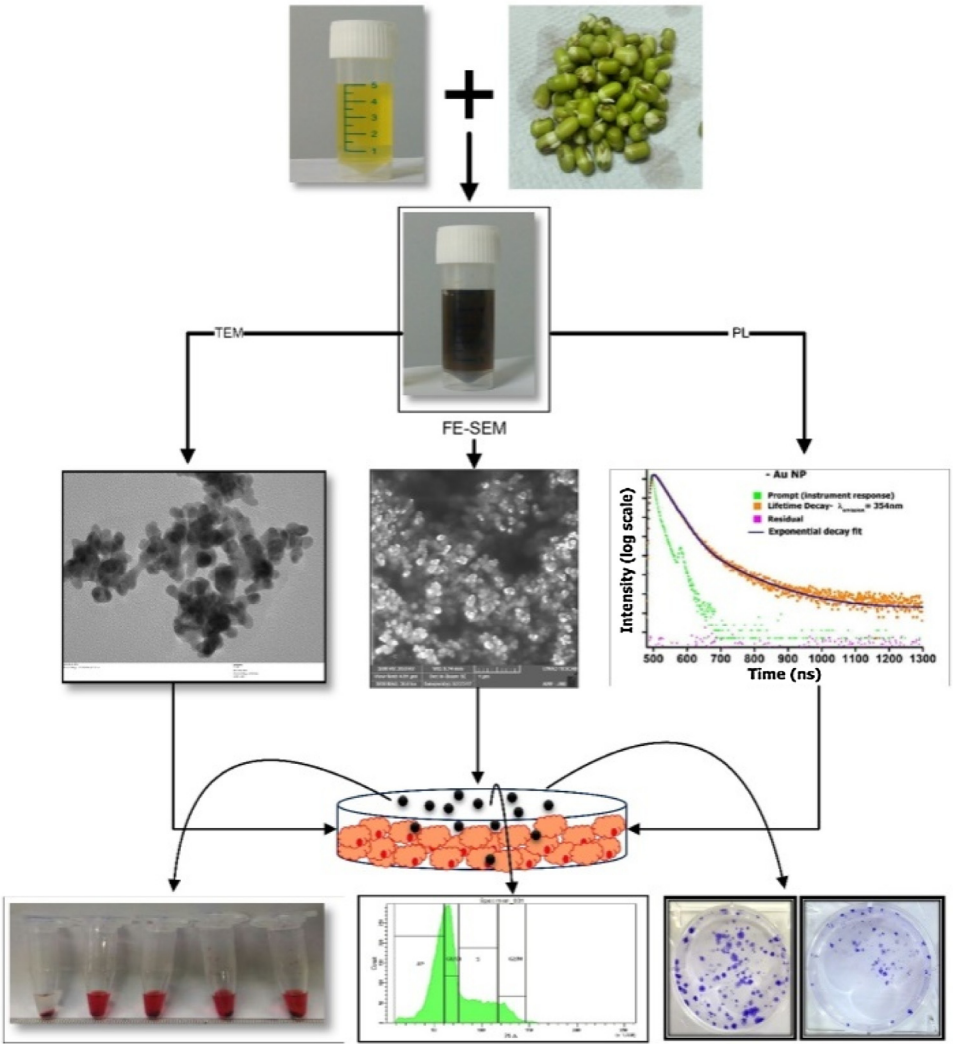

Fig. 1. Schematic representation of plan of work.

model LYRA 3 XMU]. The same sample was further used to study the elemental composition using energy dispersive X-ray fluorescence [EDXRF] spectrophotometer [PANanalytical Epsilon 5]. Moreover, 2−3 μl of the ultrasonicated sample was drop cast over a copper mesh, air-dried, and were examined by high-resolution transmission electron microscopy [JEOL 2100 F]. To further record the functional groups, present on the AuNPs surface, in the exudates, responsible for the reduction of $AuCl_4$ to form AuNPs was determined by Fourier transform infrared [FTIR] spectroscopy for this thin film of the samples was prepared on the glass slide and was scanned in the range of 600–4000 cm^{-1} using Fourier transforms infrared [FT-IR] spectroscopy [Varian 7000 FT]. Further, to study the crystalline nature of the nanoparticles X-ray diffractometer [XRD, PANalyticalX'pert PRO 2200] diffractometer with *CuKa* radiation at l = 1.5406 Å] was employed, and the sample was scanned from 0−900. The UV–vis Spectroscopy was performed using Perkin Elmer UV–vis Lambda 365 spectrophotometer in the range 200−900 nm at a step of 0.005. The photoluminescence emission spectra were obtained from an F-2700 FL Spectrophotometer using an excitation wavelength, λex = 230 nm. For structural characterization, a Rigaku mini Flex X-ray diffractometer [XRD] equipped with CuK_{α} radiation [λ = 1.54 Å] was employed, with diffraction data acquired in the range of Bragg's angle [2θ] ∼ 10–800 and at a step of 0.050.

2.4. Cell culture technique

Human Breast Cancer cell lines- MCF-7, MDA-MB-453, MDA-MB-435S, MDA-MB-231, MDA-MB-468 were procured from National Centre for Cell Science, Pune, India. The cells were grown in DMEM, L15 medium, while 10 % FBS, sodium pyruvate, penicillin-streptomycin, L-glutamine, solution was given as supplements and the cells were cultured in T-25 flasks incubated at 37 °C incubator with 5% CO2.

2.5. Membrane stability assay

The RBCs were isolated, washed with PBS [pH 7.4], centrifuged at 2000 rpm for 10 min. 2 % of the erythrocyte suspension [ES] was resuspended in [1X]PBS()1X saline solution. The volume of 1 mL reaction mixture containe 100 μL of ES, 100 μL of 0.1 % Triton X-100 and 25, 50, or 100 μg/mL of AuNPs in Eppendorf tubes. This was incubated for 60 min at 37 °C under constant agitation and then centrifuged at 2000 rpm for 10 min after that 250 μL of the supernatant was plated in 96-well plate. Then, the release of hemoglobin was determined by photometric analysis of the supernatant at 576 nm in a multiplate reader. Complete hemolysis was achieved by using 0.1 % Triton X-100 [positive control] yielding 100 % hemolysis and PBS [negative control] yielding 0 % hemolysis [11].

2.6. PBMC isolation

For this human blood with an anti-coagulant citrate buffer solution and was diluted with a phosphate buffer saline[PBS] [v/v 1:1]. 3 mL Histopaque [1.07 g ml^{-1}] was taken in a centrifuge tube and was tipped on the histopaque layer. Subsequently, it was centrifuged at 400 g for 30 min and lymphocytes were collected from the buffy layer. The isolated lymphocytes were then washed thrice with 2 mL PBS followed by 2 mL RPMI-1640 media through centrifugation steps separately for 10 min at 250 g. The lymphocytes pellets were then suspended in RPMI-1640. Cells were suspended in RPMI-1640 and 2×10^3 cells were seeded in 96 well plates with supplementation of 10 % heat-inactivated FBS. Initially, cells were incubated at 37 °C in 5% CO2 for 8 h in RPMI-1640 without FBS.

2.7. Cytotoxicity of AuNPs by MTT and Alamar blue assay

Biogenic AuNPs mediated cytotoxicity on breast cancer cells was determined by thiazolyl blue tetrazolium bromide MTT assay as described in Saikia et al. [12] with slight modification. Breast cancer cells MCF-7, MDA-MB-453, MDA-MB-435S, MDA-MB-231, MDA-MB-468 were seeded in 96-well plate at the cell density of 2×10^3 cells per well and treated with increasing concentrations [25, 50, 100 μg/mL] of AuNPs for 48 h at 37 °C, 5% CO2. Before termination of the experiment, 20 μl of [5 mg/mL] MTT reagent was added to each well, and the plate was sustained at 37 °C in the incubator for 2 h. After aspirating the supernatant, 200 μl of dimethyl sulfoxide [DMSO] was added to each well to solubilize the formazan crystals formed in viable cells. The optical density [OD] was spectrophotometrically measured at 570 and 690 nm. For Alamar Blue Assay, after completion of the stipulated time period, cells were washed twice with PBS prior to the addition of Alamar Blue [5 % w/v in PBS]. Kept for 4 h of incubation, fluorescence was measured with a fluorescence spectrophotometer at excited wavelengths of 570/600 nm.

2.8. Cell viability assay

The cell viability was determined using the trypan blue exclusion assay in MCF-7 where cells were seeded in 25 mm petri-dish and treated with 25, 50 and 100 μg/mL of AuNPs for 48 h at 37 °C, 5% CO2. The cells were trypsinized and stained with trypan blue [0.4 % in PBS], and scored under a light microscope by hemocytometer according to the number of viable cells remains unstained to the dead population stained with trypan blue.

2.9. Flow cytometric analysis

The cells were stained with a fluorescent dye, propidium iodide [PI], which binds to the DNA in a stoichiometric manner as it's been known that there is a direct relationship between DNA content and PI fluorescence. Flow cytometric analysis was done as described by Riccardi and Nicoletti [13]. Briefly, MCF-7 cells [1×10^5 cells/well] were treated with various concentrations [25, 50, and 100 μg/mL] of AuNPs. After 48 h of incubation, both adherent and floating cells were collected by trypsinization, washed twice with ice-cold PBS, fixed in ice-cold 70 % methanol for overnight at -20 °C and subsequently incubated with PI [20 μg/mL] and RNase A [200 μg/mL] for another 30 min at 37 °C. Cell cycle distribution was then analyzed by flow cytometer [BD FACS LSR III, BD Biosciences, USA]. Finally, the percentage of cells in different phases of the cell cycle was determined by BD Diva software.

2.10. Colony forming assay

To assess the colony-forming ability of gold nanoparticle, whether treated or untreated MCF-7 breast cancer cells were incubated for 2 weeks. MCF-7 breast cancer cells were seeded with media containing AuNPs at various concentrations of 25 μg/mL, 50 μg/mL, and 100 μg/mL in triplicate on a 6-well tissue culture plate with 1000 cells/well. Following 14 days incubation at 37 °C colonies were fixed [ethanol to acetic acid, 3:1] and stained with 0.5 % crystal violet in methanol, later the number of colonies was counted. For all the experiments performed, control cells remained untreated and kept for the same duration as the longest time point of the respective experiment(ref).

2.11. Statistical analysis

All the results were presented as Mean ± SEM. Statistical analysis was performed using ANOVA following Mann-Whitney *U* test A value of $p \leq 0.001$, $p \leq 0.01$ and $p \leq 0.05$ was considered as significant difference between the compared groups.

3. Results

3.1. Physical characterization

3.1.1. X-Ray diffraction [XRD] analysis

Biogenic AuNPs were subjected to XRD analysis to obtain relative information regarding crystal nature. The prepared nanoparticles were found to be composed of crystals in the cubic phase. The resultant XRD diffractogram Fig. 2[a] showed characteristic peaks located at ~38.180, 44.390, 64.580, 77.550, corresponding to lattice planes-[111], [200], [220] and [311] respectively [JCPDS-ICDD 1999; JCPDS No. 04-0784]. The peak corresponding to [111] plane is found to be most intense suggesting that [111] may the predominant orientation for crystal growth. The crystallite size, d, of the [111] peak being the most prominent peak, was calculated using Debye-Scherrer's equation [Eq. 1], and was found to be 12.6 nm, the lattice parameter being 4.08 A°.

$$d = \frac{k\lambda}{\beta cos\theta} \quad (1)$$

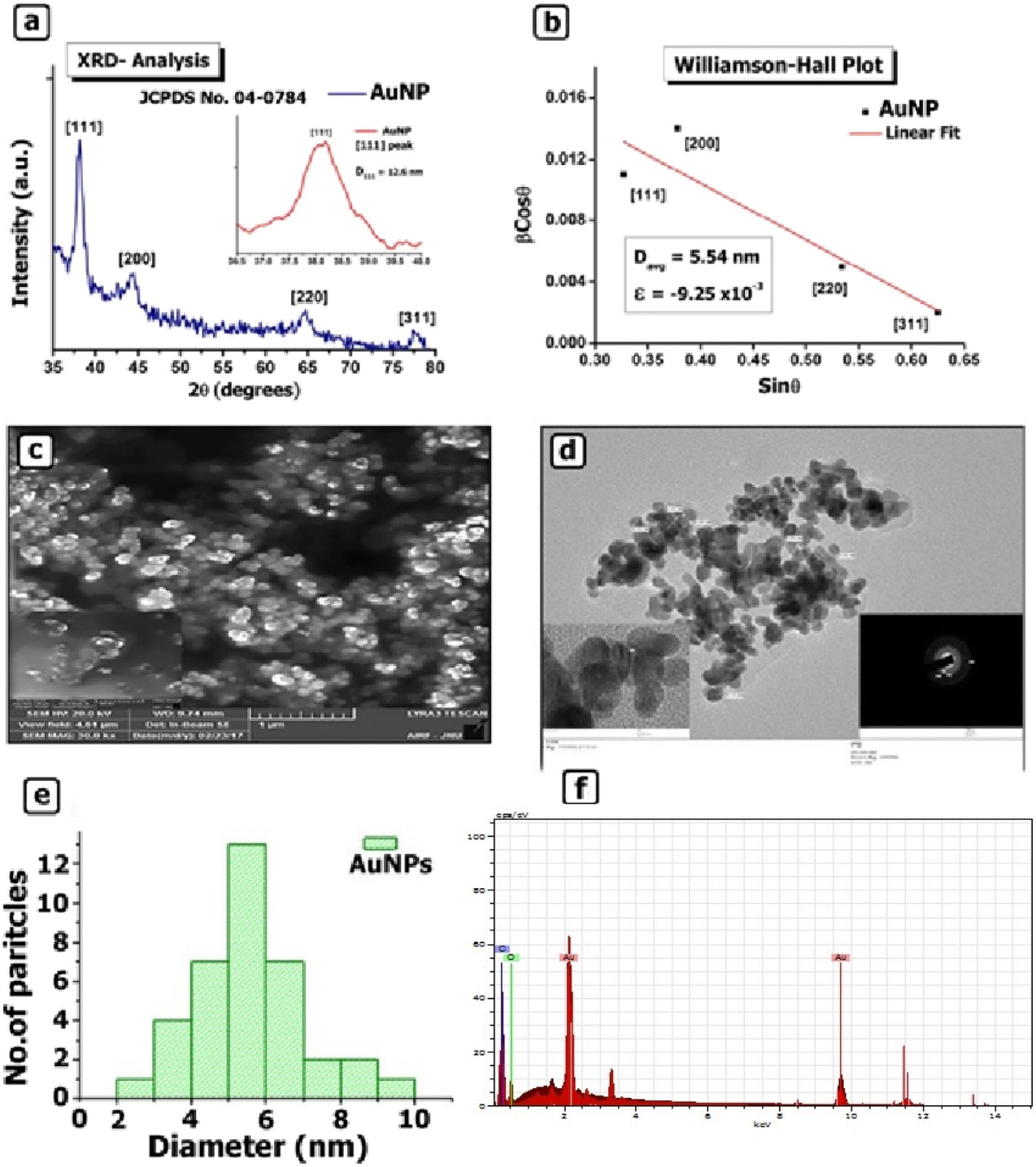

Fig. 2. The XRD diffractograph is shown in [a] with the most prominent peak corresponding to the plane [111] according to ICDD with the Williamson-Hall plot shown in [b] used to determine the average crystallite size and the microstrain developed in the crystal lattice. The FE-SEM image is shown in [c] with [d] depicting the TEM images with insets of SAED pattern. The histograph for the size distribution is given in [e] and [f] Exhibit EDX of the synthesized AuNPs.

In Eq. 1, k is the dimensional constant depending on the particular geometry of the scattering object∼ 0.9, λ is the wavelength of the incident X-ray source and b is the full-width half maxima of the [111] peak calculated using Origin 8.5. The average crystallite size was determined to be ∼5.54 nm using the Williamson-Hall plot, Fig. 2[b], also revealing a negative micro-strain developed in the lattice system.

3.1.2. Morphological study

3.1.2.1. FE-SEM imaging. FE-SEM was conducted to obtain the micrograph of biogenic AuNPs as shown in Fig. 2[c]. Image revealed that AuNPs surface is smooth and spherical in shape. EDX is very useful to identify the elemental status or chemical composition of the sample illustrated in Fig. 2[f]. Presence of a strong peak of approximately at 2.1 keV confirmed the elemental nanocrystalline AuNPs.

3.1.2.2. TEM imaging. Morphological characteristic was done by means of high-resolution transmission electron microscopy [HR-TEM]. Study revealed that biogenic AuNPs are mostly spherical in nature and size falls mostly in the range of 4–10 nm with the tendency to aggregates as shown in Fig. 2[d]. The difference in size and shape of biogenic may be due to the differential growth pattern of AuNPs. Selected area electron diffraction [SAED] pattern showed in the inset of Fig. 2[d] exhibited four spectral ring which correspond to [1 1 1], [2 0 0], [2 2 0] and [3 1 1] related with SAED pattern as documented, to authenticate the crystalline nature of the nanoparticles.

3.1.2.3. Spectroscopic analysis UV–vis spectroscopy analysis. AuNPs are known to exhibit surface plasmon resonance [SPR], arising from an interacting electromagnetic field induced collective free conduction electrons oscillation [14]. The width, position, and a number of SPR bands optical absorption spectra, is usually sensitive to the cluster size and shape, local refractive index as well as particle medium interaction. The AuNPs formation was clearly identified by the distinctive surface plasmon resonance [SPR] band centered at 548 nm. Spherical particles have only one SPR, this band is generally overlapped by absorption which originates from transitions, namely by single electron-optical excitations from the occupied 5d band to the unoccupied levels of the 6s-6p band of the metal [15–17]. Thus, the SPR peak can also be utilized not only to determine the particle size for a UV–vis spectrum under ∼600 nm but also the shape of the particle. However, certain calculations lead to an error of ∼6–25 % [18–21]. The average particle was calculated using the effective mass approximation [6] given by Eq.2.

$$\boldsymbol{r(nm)} = \left[\left\{\frac{-0.2963 + \left(-40.197 + \frac{13620}{\lambda_p}\right)}{-7.34 + \frac{2418.6}{\lambda_p}}\right\}\right]^2 \quad (2)$$

Using Eq.2, and utilizing the SPR band peak ∼548 nm, calculated average obtained particle size r∼5.34 nm which is in good agreement to that found from the Williamson Hall plot. Optical absorption measurements are widely used to understand the band-gap [22,23]. The optical band-gap of the AuNPs system was also determined using the Tauc Plot Fig. 3 [b]. Tauc model is the most widespread method which allows us to derive the band-gap

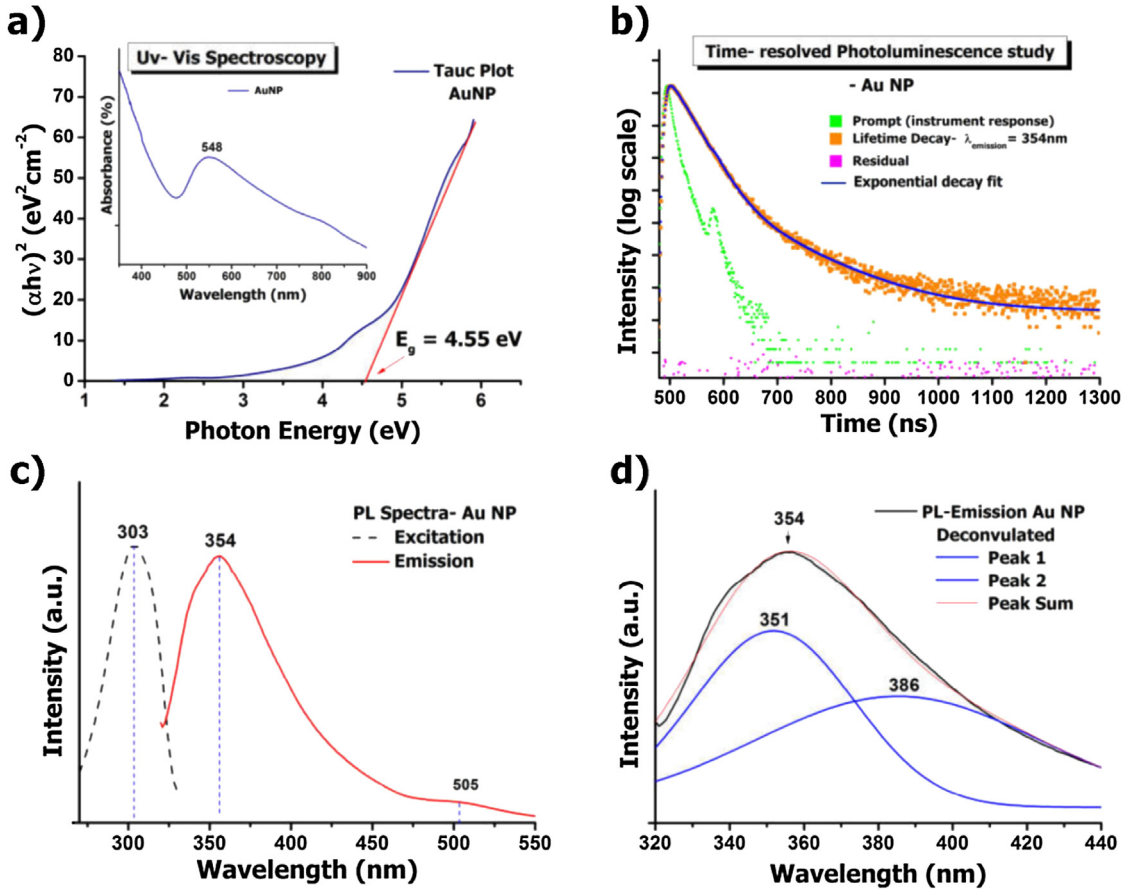

Fig. 3. The Tauc plot for determination of the energy band gap of the AuNP system is shown in [a] with inset depicting the entire absorbance response with peak shown at 548 nm. The TRPL response for the emission peak at 354 nm is shown in [b]. PL response is shown in [c] with the excitation as well as emission spectra and the peak at 354 has been de-convulated [d].

energy Eg as a function of the incident energy E. The absorption coefficient, 'α'was determined using the well-known Beer's law given by Eq.3, neglecting the reflectance term:

$$\boldsymbol{\alpha} = \frac{\ln\left\{\frac{100}{\%T}\right\}}{\boldsymbol{d}} \quad (3)$$

In Eq.3, % T is the transmittance, which is determined using Eq. 4:

$$\boldsymbol{A} = 2 - \boldsymbol{log}_{10}(\boldsymbol{\%T}) \quad (4)$$

In Eq 4, 'A' is the absorbance or optical density as observed from the spectrum. The optical band- gap hence found for the AuNP is 4.55 eV.

3.1.2.4. Photoluminance study. The photoluminescent behavior of Au NPs can give information about the structure and influence of the ligands on metal cores. Moreover, this is an interesting property for the use of AuNPs as biomarkers. Fig. 3 [c] displays room temperature PL spectra of the Au NP excited at a wavelength of 300 nm exhibiting strong emission at 354 nm and a broad characteristic visible peak centered at 505 nm. This excitation wavelength has been selected on the basis of the excitation spectra.

3.1.2.5. Fourier-transform infra-red spectroscopy [FTIR]. The presence of biomolecules with functional groups present in the seed exudates having the potential for the reduction of gold ions into nanoparticles and their stability was analyzed using FTIR spectra at diverse vibrational stretches in the range of 600–4000 cm^{-1} [Fig.4].

Where the analytical peaks, stretching, vibration revealed the presence of different functional groups, such as peak at 765 cm^{-1} attributed to aliphatic chloro-compounds [C–Cl] bond, Another band at 917 cm^{-1} may be attributed to —CH=CH2 bonds. The bands at 1486 cm^{-1} C=C stretching vibration. The IR bands observed at 1571 and 1742 cm^{-1} may be assigned to —C—H — stretching and —C=O—stretching modes, respectively. However, the band observed at 2384 and 3502 cm^{-1} may be due to the presence of —C≡C—and Hydrogen bonding respectively [37].

3.2. Characterization

3.2.1. Cytotoxicity of AuNP on PBMCcells

To assess the cytotoxicity of AuNPs in contrast to PBMC cells, MTT and Alamar blue assay were performed, where PBMCs cells were treated with various concentration of AuNPs for 24 h. In both the assays, No significant cytotoxic effect was observed in the PBMC even at the highest concentration [100 μg/mL] as compared to control as shown in Fig. 5[a] and [b] by MTT and Alamar Blue respectively.

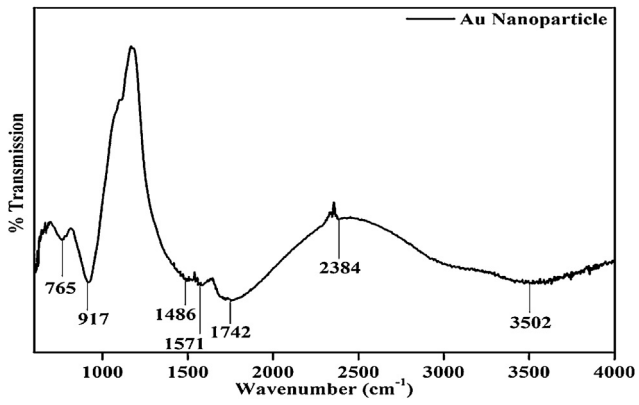

Fig. 4. FTIR spectrum of biogenically synthesized AuNPs.

3.2.2. Membrane stability test

The results for the membrane stability assay in terms of the percentage of hemolysis are shown in Fig. 5 **[c].** It was found to be 0.046 % in case of the negative control PBS, and 100 % in case of the positive control Triton X-100. Whereas, in case of AuNPs it was found to be 77.56 % for 25 μg/mL, which differ significantly at $p \leq 0.01$ with the positive control; and 76.02 % and 65.88 % for 50 μg/mL and 100 μg/mL respectively, with significant difference [$p \leq 0.001$] with the positive control. Hence it was seen that up to the studied concentrations, the surface functionalization of AuNPs conferred stability to the red blood cells and prevented hemolysis to a considerable extent. Therefore, the membrane stability retained even at high concentration of AuNPs. Triton X-100 is generally used to lyse cells or to permeabilize the membranes of living cells. It was observed that in the presence of AuNPs, Triton X-100 exhibited significantly less hemolysis than the pristine samples.

3.2.3. Cytotoxicity of AuNP on breast cancer cells

Cytotoxicity of biogenic AuNPs was tested using MTT and Alamar blue assay against breast cancer cells MCF-7, MDA-MB-453, MDA-MB-435S, MDA-MB-231, and MDA-MB-468, with various concentration [25, 50 and 100 μg/mL] of AuNPs for 48 h [Fig. 6]. Thus, the cytotoxicity results revealed that the biogenic AuNPs significantly induce toxicity with the increasing dose of nanoparticles indicating anticancer activity in dose dependent manner.

3.2.4. Cell viability assay

To determine the cytotoxic effect of AuNPs on MCF-7 cells, cell viability assay was performed using the trypan blue dye exclusion method. Cells were treated with various doses of [25, 50, and 100 μg/mL], and its effect on live and dead cell number was calculated after at the end of 48 h. Using the trypan blue, we observed that the decrease in total cell number is accompanied by an increase in significant cell death thus corroborating the MTT results as shown in **[**Fig. 7].

3.2.5. Cell-cycle analysis

To assess the effect of bio-synthesized AuNPs on cell cycle progression, performed on MCF-7 breast cancer cell lines using propidium iodide(PI) as a staining agent, where cells are exposed to various concentrations of AuNPs [25, 50 and 100 μg/mL], after 48 h of treatment, cell cycle was analyzed. Present Study revealed that cell cycle arrest was observed at G2/M phase with the increasing dose of nanoparticles showed a marked increase in apoptotic phase at high dose [100 μg/mL] of AuNP as compared to control ($p \leq 0.001$) [Fig. 8].

3.2.6. Clonogenic assay

The results indicated that the clonogenic capacity of MCF-7 cells was reduced in a dose-dependent manner as at higher concentrations the number of colonies, plating efficiency, and surviving fraction was greatly reduced as compared to control cells on 14 days of continuous exposure. Data have shown that there was a significant dose-dependent inhibition of clonogenic survival from ∼[25−1.3%] [$p \leq 0.001$] for MCF-7 cells as compared to control. Bar graph indicated that there were almost diminished the Survival fraction [SF] and plating Efficiency [PE] at a higher dose of AuNPs treatment [Fig. 9].

4. Discussion

The dependency of humans on nanomaterial is not new as they are being used in "*bhasmas*", evidenced from ancient Indian medicinal literature particularly silver, gold, etc. [24]. These nanomaterials can be synthesized through various means broadly,

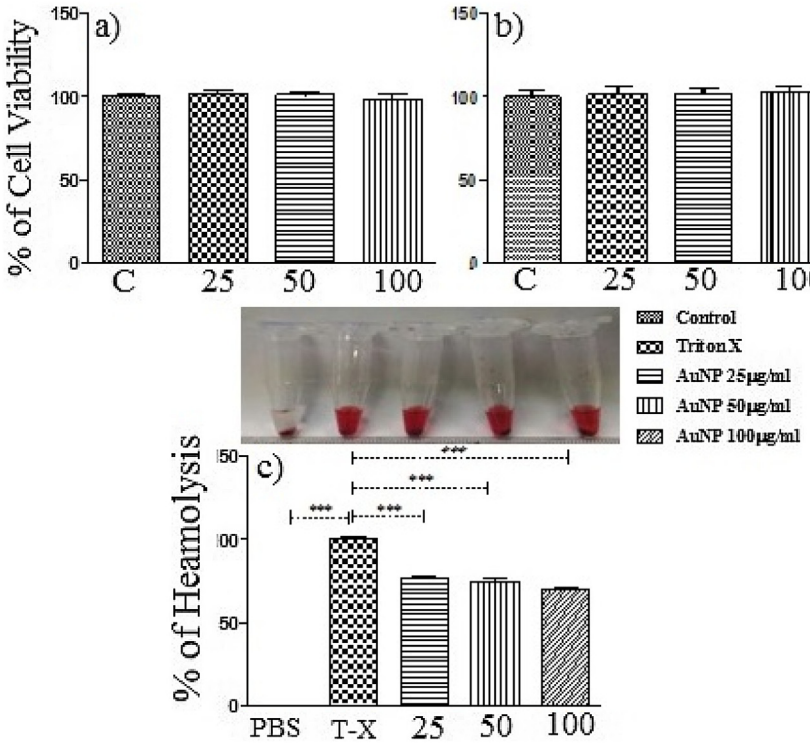

Fig. 5. a] Cytotoxic assay though MTT on PBMCs, b) Cytotoxic assay though Alamar blue on PBMC c) Membrane stability assay of AuNPs on PBMCs. Data are expressed as mean ± SE [n = 3]. ***significant $p < 0.001$.

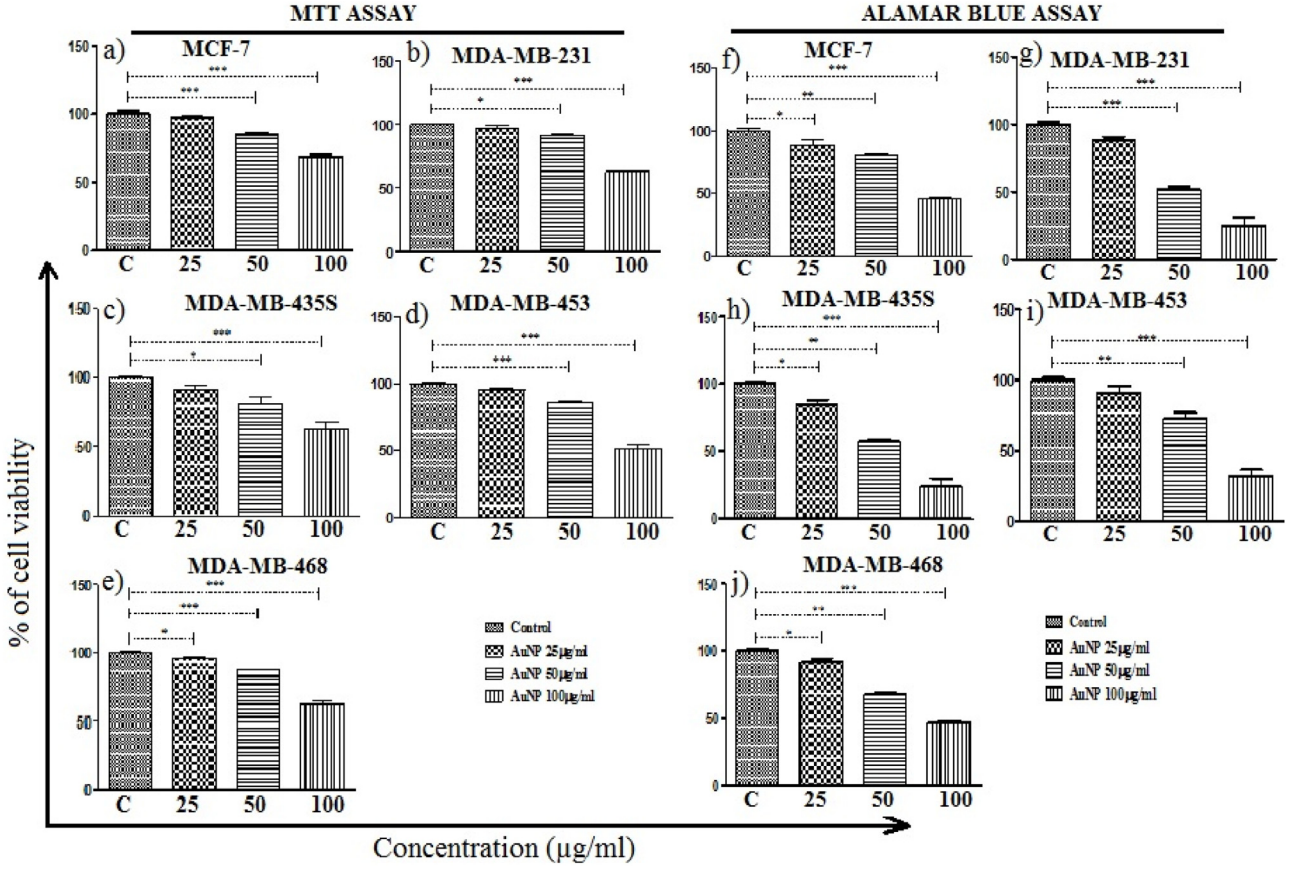

Fig. 6. Cytotoxic assessment through MTT and Alamar blue assay on various breast cancer cell lines exposed to biogenic AuNPs- [a, f] MCF-7, [b, g] MDA MB435 s, [c, h] MDA MB 231 [d, i] MDA MB 468 [e, j] MCF7. Data are expressed as mean ± SE [n = 3]. * significant $p < 0.05$, ** significant $p < 0.01$, *** very significant $p < 0.001$.

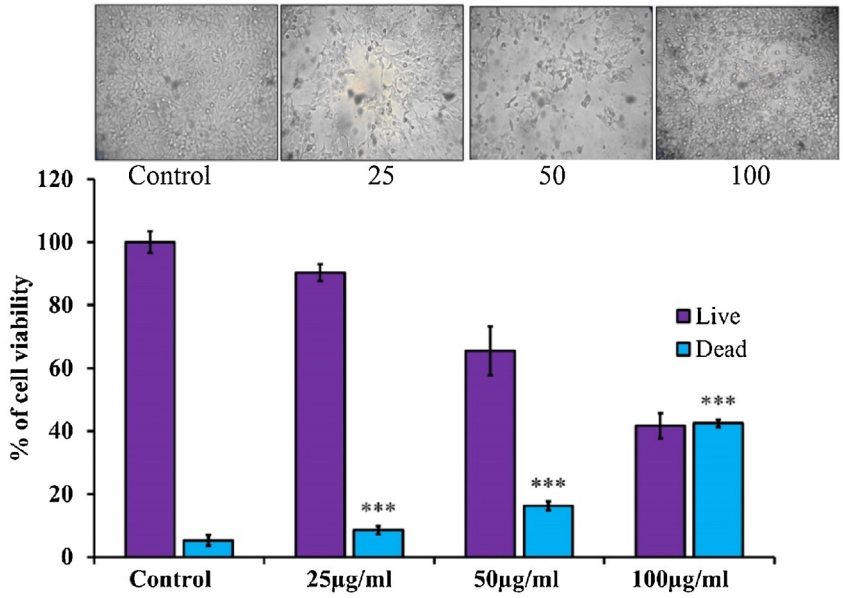

Fig. 7. Cell viability assay on MCF-7 using trypan exclusion method.

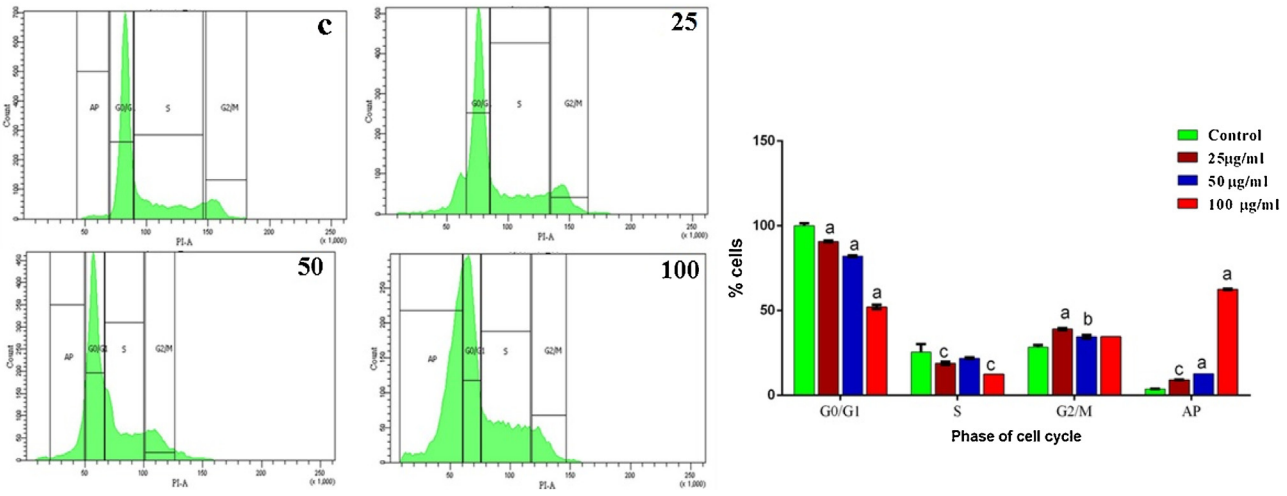

Fig. 8. Flow cytometry analysis of cell cycle phase distribution in MCF-7 cells. Bar diagram showing the cell distribution in the subG1, G0/G1, S and G2/M phases for MCF-7 cells treated with vehicle control and AuNPs [25, 50 and 100 μg/mL]. Data are expressed as mean ± SEM [n = 3]. c = $p < 0.05$, b = $p < 0.01$ a = $p < 0.001$ vs control group.

chemically, physically, or biologically. However, the synthesis of nanomaterial through chemical and physical means are not only costly but also use harmful chemicals leaving behind a trail of toxic by-products. Therefore, time to move towards the technology which is not only cost-effective but also free from hazardous chemicals and are biocompatible, such as "green nanotechnology" thus, minimizing the potential risks induced on both humans and environment during the synthesis of nanomaterial. Various research across the world confirmed nanoparticles synthesis using various biological ranging from fungi to plants, exhibiting there anticancer potential [25–28].

Mung bean (*Vigna radiata)*, an important pulse being commonly consumed in different countries specially in asian countries as daily protein requirement, like sprouts and found to exhibit various biological activities such as antioxidant effects, antimicrobial activity, antipyretic activities including antitumor activities, which may be due to the presence of various phytochemicals found in seed and its sprouts such as Apigenin, Genistein, Vitexin, Naringin, Gallic acid, etc. [29]. In this line synthesis of biogenic AuNPs using seed exudates of *Vigna radiata* was investigated followed by its therapeutic application was studied through anticancerous potential using various breast cancer cell lines.

During the process of germination its chemical constituents undergo series of changes biochemically, the process of imbibition causes seepage of various compounds into the exudate, these phytochemicals found in the exudate serves to exhibit antimicrobial and antioxidant properties which might be responsible for the reduction of AuCl2 to AuNPs. Common free phenolics found in green gram seed exudate are sinapic, ferulic, and gallic acid [30]. Thus, synthesized AuNPs examined through various characterization techniques [SEM, TEM, UV–vis spectroscopy, FTIR, XRD, etc.] unveiling their unique feature such as shape, size, crystallinity, functional groups present of the surface of biosynthesized nanomaterial.

The crystalline nature of AuNPs synthesized from the seed exudates was analyzed using the X-ray diffraction studies

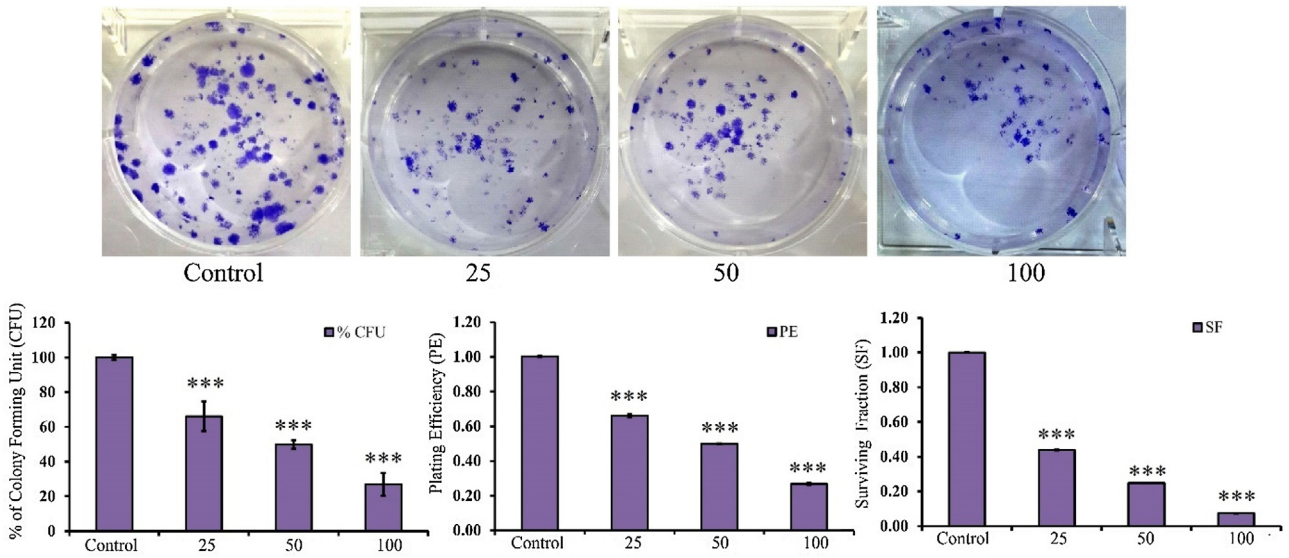

Fig. 9. Effect of Biogenic AuNPs on colonogenecity inhibition on MCF-7 cells. a] Colony formation unit b] plating efficiencyandc]surviving fraction was analyzed and representative pictures are shown in the upper panel. Data expressed as [Mean ± SEM, n = 3]. Values are significant where * signifies $p < 0.05$, ** signifies $p < 0.01$, *** signifies $p < 0.001$ as compared with the control.

revealing the peaks at 111, 200, and 220. These findings are supported by earlier studies on gold nanoparticles where they reported crystalline nature and similar peaks as observed in the present study [31].

FE-SEM image revealed smooth round surface morphology of the synthesized nanoparticles, however, synthesized gold species is confirmed by the EDX analysis, where AU peaks confirm the presence of gold element in the sample whereas C peak may be due to the usage supporting film over which sample was placed on similar observation reported by Nagalingam et al. [32]. Further, Transmission electron microscopy [TEM] image depicted in [Fig. 3a and b] revealed the shape and size of the nanoparticles. Obtained morphology for gold nanoparticles from seed exudateswas found to be spherical to pseudo spherical shaped. Whereas the contrasting light region around the dark region might be due to the adsorbed organic compound leading to its reduction and its stabilization. Inset SAED pattern of synthesized nanoparticles confirms its crystal nature; the results are also supported by Kajani et al., [33] has been reported that the gold nanoparticles were reduced using *Taxus baccata* [33]. Further the size of the gold nanoparticles ranged between 2–10 nm and is seen non–agglomerated due to the capping of bio-organic compounds present in the seed exudates however most of them fall in the range of 4–6 nm as shown in the histogram. Altogether, the seed exudates act as a ligand that stabilizes gold nanoparticles, in line with another study which concluded that the role of the bio-organic compound found in seaweeds acts as reducing and stabilizing agents [34]. However, there are no precise mechanisms that explain the formation of different shapes of gold nanoparticles.

Further elemental composition of the biogenically synthesized AuNPs was analyzed through EDX, results revealed that synthesized AuNPs peak was found in between the range of 2–4 along with C and O peaks might be due to the presence of phytoconstituents mediated reduction of gold nanoparticles. A similar kind of observation was reported by by Balashanmugam et al., [35].

UV–vis spectroscopy was performed which is the most commonly used technique for their optical characterization because the absorption band depicts the aspect ratio and diameter of the nanoparticles providing primary information about the size of the nanoparticle. As shown in Fig. 3, the SPR peak hight centered at 548 nm confirms AuNPs synthesis. it is similar to the results reported by Kamal et al., [36].The FTIR spectra of biogenic gold nanoparticles are shown in Fig. 4. To identify the possible bio-organic molecules responsible for the stabilization of gold nanoparticles. FT-IR spectroscopic analysis was conducted based on the literature survey revealed that the seed exudates are found to be rich in biomolecules that are responsible for the reduction of metallic ions into nanoparticles [37]. The peak at 765 cm^{-1} attributed to aliphatic chloro-compounds [C—Cl] bond, Another band at 917 cm^{-1} may be attributed to —CH=CH2 bonds. The bands at 1486 cm^{-1} C=C stretching vibration. The IR bands observed at 1571 and 1742 cm^{-1} may be assigned to —C—H— stretching and —C=O—stretching modes, respectively. However, A similar pattern of observation can be seen where the band observed at 2384 and 3502 cm^{-1} may be due to the presence of —C≡C— and Hydrogen bonding respectively [38].

In the case of PBMCs, where no negative effect was observed on normal human PBMCs even at various doses of AuNP synchronized with another study where phytoreducedAuNP showed no toxicity on peripheral lymphocytes whereas anticancer activity was found when A549 cells were treated with bio-reducedAuNP [39,40]. Interestingly, nanomaterial exposed RBCs in the presence of Triton-X-100 promotes membrane stability in contrast to those exposed to Triton-X-100 only. This may be due to the physico-chemical property of nanomaterial, which majorly decides their behavior and further their interaction with the various component of the cell in the biological milieu. the results of cytotoxicity assay on PBMC showed that AuNPs did not produce any substantial cytotoxicity and were found safe in the tested concentration. Further, the therapeutic applications of biogenic AuNPs were carried out by MTT and Alamar assay for its anticancer potentials against various breast cancer cell lines viz. MCF-7, MDA-MB-231, MDA-MB-435S, MDA-MB-453, MDA-MB-468. The present investigation revealed their anticancer potential against the exposed breast cancer line. The results presented here indicate that biogenic AuNPs showed a typical dose-response behavior observed in all cell lines tested, however, MCF-7 showed more effective anticancer potential of the extract. Our study is in consistent with the studies conducted by the various research group, showing the anticancer property as biosynthesized gold nanoparticles using

Anacardium occidentale leaves extract against MCF-7 cells, and using flower extract of *C. guianensis* against HL60 cells [40,41]. However the cytotoxic effect of gold nanoparticles has been reported on various studies where they exhibit selective anticancer activity against the exposed cell lines this might be due to the attachment of plant components on the surface of nanoparticles [39–42]. From the trypan blue exclusion method, the present study reveals that AuNPs showed extensive inhibition of cell growth. Thus exhibiting its cytotoxic effect on MCF-7 cells and validating the MTT results. Similar results were observed by Nindawat and Agrawal [43], where biologically reduced silver nanoparticles cause a cytotoxic effect on HeLa cells. Based on the present investigation it may be concluded that the AuNPs are non-toxic to normal cells but it has the potential to selectively arrest the growth of cancer cells, however it needs a further concrete study to validate these facts.

Therefore, biogenic AuNPs were subjected for further assessment of cellular toxicity for validation by measuring the DNA distribution in various phases of the cell cycle through Flow cytometry analysis on MCF-7 cells. Biogenic AuNPs might suppress DNA replication and eventually arrest the cells in S and G2/M phase of cell cycle evidenced by accumulating cell number at 48 h. A similar observation was reported by earlier studies on MCF-7 and S phase arrest in MDA-MB-231. Cell cycle arrest was reported when MCF-7 cells were exposed to *Euphorbia hirta* extract [44–46].

The clonogenic assay is a method to determine the effectiveness of cell reproductive death after treatment with cytotoxic agents, only a fraction of seeded cells retain the capacity to produce colonies. The capacity for continued proliferation characteristic of cells in tissues is essential for the continued integrity and function of cancer cells that lead to cause disease aggressiveness. Thereby, modulation of this capacity for clonogenicity is one the strategy for tumor eradication and also required for the prevention of recurrence of the diseases.

The results of the present clonogenic study on MCF-7 cells revealed that as the dose-dependent clonogenic capacity was decreased, plating efficiency [PE = Ratio of the number of colonies/ number of cells seeded] and surviving fraction [SF = is a function of dose determined using] were also found to decrease with increasing dosage of biogenically synthesized AuNPs, present result was in agreement with the study performed by Nindawat and Agrawal [42] where exposure of biologically reduced AgNPs using *Arnebia hispidissima* causes a dose-dependent decrease in HeLa cells colony formation and surviving fraction which might be due to induction of apoptosis, chromosomes damage, etc., [42].

Overall the seed exudates might act as a ligand that stabilizes gold nanoparticles. However, there are no precise mechanisms that explain the formation of different shapes of gold nanoparticles. As biogenic gold nanoparticles are known biocompatible, non-toxic compounds, therefore, observed anticancer activity on the tested breast cancer cell lines might be due to the release of phytochemicals in the exudate which is being adsorbed on the surface of AuNP referencing their anticancer and anti-proliferative potential against the cell line. Common free phenolics found in green gram seed exudate are sinapic, ferulic, and gallic acid [30]. Gallic acid [GA] also found in mung bean known for potent anticancer activity against various cell lines such as A549 [46,47,49]. However further study is required to elucidate molecular mechanism behind their anticancer potential also whether the biosynthesized nanomaterial can be used for drug delivery or not.

5. Conclusion

From the results it may be concluded that various analytical techniques (UV absorption spectrum, SEM, EDX, XRD, and HR-TEM) reveal characteristic property confirming the biogenic synthesis of AuNPs from Vigna radiata (moong bean) seed exudates, demonstrating size and shape of NPs. Further, Phytoconstituents of moong bean seed exudate not only play a vital role in stabilizing the gold nanoparticles but, found to be cytotoxic to the studied breast cancer cells. However, no side effect has been observed in the normal human PBMCs. Furthermore, the cell cycle arrest of cancer cell lines at the G2/M stage and promoting cells to undergo apoptosis, at the highest exposed dose. Among the various physicochemical study, present AuNPs shows unique information, they show photoluminescent property which may be used for bioimaging purposes.

Transparency document

The Transparency document associated with this article can be found in the online version.

Declaration of Competing Interest

Authors declared no conflict of Interest.

Acknowledgments

NS and MKD thanks the UGC (university Grant Commission), New Delhi, India for providing fellowship BSR and RGNF. AIRF, JNU for their electron microscopy facility is acknowledged.

Appendix A. Supplementary data

Supplementary material related to this article can be found, in the online version, at doi:https://doi.org/10.1016/j.btre.2021.e00612.

References

[1] D.L. Holliday, V. Speirs, Choosing the right cell line for breast cancer research, Breast Cancer Res. 13 (4) (2011) 215.
[2] J. Akhtar Siddiqui, et al., Phytochemicals for breast cancer therapy: current status and future implications, Curr. Cancer Drug Targets 15 (2) (2015) 116–135.
[3] B. Sun, N. Hu, L. Han, Y. Pi, Y. Gao, K. Chen, Anticancer activity of green synthesised gold nanoparticles from Marsdeniatenacissima inhibits A549 cell proliferation through the apoptotic pathway, Artif. Cells Nanomed. Biotechnol. 47 (1) (2019) 4012–4019.
[4] W. Cai, et al., Applications of gold nanoparticles in cancer nanotechnology, Nanotechnol. Sci. Appl. 1 (2008) 17.
[5] M. Cinelli, et al., A green chemistry-based classification model for the synthesis of silver nanoparticles, Green Chem. 17 (5) (2015) 2825–2839.
[6] R. Bhosale, et al., Innovative eco-friendly approaches for green synthesis of silver nanoparticles, Int. J. Pharm. Sci. Nanotechnol. 7 (1) (2014) 2328–2337.
[7] R. Liu, Q. Pei, T. Shou, W. Zhang, J. Hu, W. Li, Apoptotic effect of green synthesized gold nanoparticles from Curcuma wenyujin extract against human renal cell carcinoma A498 cells, Int. J. Nanomed. 14 (2019) 4091.
[8] R. Geetha, T. Ashokkumar, S. Tamilselvan, K. Govindaraju, M. Sadiq, G. Singaravelu, Green synthesis of gold nanoparticles and their anticancer activity, Cancer Nanotechnol. 4 (4–5) (2013) 91–98.
[9] Z. Yun, A. Chinnathambi, S.A. Alharbi, Z. Jin, Biosynthesis of gold nanoparticles using Vetex negundo and evaluation of pro-apoptotic effect on human gastric cancer cell lines, J. Photochem. Photobiol. B, Biol. 203 (2020)111749.
[10] K. Ganesan, B. Xu, A critical review on phytochemical profile and health promoting effects of mung bean [Vigna radiata], Food Sci. Hum. Wellness 7 (1) (2018) 11–33.
[11] R. Borah, A. Kumar, M.K. Das, A. Ramteke, Surface functionalization-induced enhancement in surface properties and biocompatibility of polyaniline nanofibers, RSC Advances 5 (60) (2015) 48971–48982.
[12] C. Saikia, M.K. Das, A. Ramteke, T.K. Maji, Effect of crosslinker on drug delivery properties of curcumin loaded starch coated iron oxide nanoparticles, Int. J. Biol. Macromol. 93 (2016) 1121–1132.
[13] C. Riccardi, I. Nicoletti, Analysis of apoptosis by propidium iodide staining and flow cytometry, Nat. Protoc. 1 (3) (2006) 1458–1461.
[14] F. Toderas, M. Iosin, S. Astilean, Luminescence properties of gold nanorods, Nucl. Instrum. Methods Phys. Res. B 267 (2) (2009) 400–402.
[15] W. Krasser, J. Tiggesbaumker, Uwe Kreibig and Michael Vollmer: Optical Properties of Metal Clusters, Springer Verlag, Berlin, 1995, pp. 532 ISBN 3-540-

57836-6P, r eis: 98,-DM. Berichte der Bunsengesellschaft für physikalische Chemie, 1997. 101[5]: p. 878-878.
[16] Y. Xia, N.J. Halas, Shape-controlled synthesis and surface plasmonic properties of metallic nanostructures, MRS Bull. 30 (5) (2005) 338–348.
[17] V. Amendola, et al., Self-healing of gold nanoparticles in the presence of zinc phthalocyanines and their very efficient nonlinear absorption performances, J. Phys. Chem. C 113 (20) (2009) 8688–8695.
[18] W. Haiss, et al., Determination of size and concentration of gold nanoparticles from UV− Vis spectra, Anal. Chem. 79 (11) (2007) 4215–4221.
[19] C.J. Murphy, et al., Anisotropic Metal Nanoparticles: Synthesis, Assembly, and Optical Applications, ACS Publications, 2005.
[20] V. Bogatyrev, et al., Differential light scattering spectroscopy for studying biospecific assembling of gold nanoparticles with protein or oligonucleotide probes, Colloid J. 64 (6) (2002) 671–680.
[21] W. Rechberger, et al., Optical properties of two interacting gold nanoparticles, Opt. Commun. 220 (1–3) (2003) 137–141.
[22] C.G. Ribbing, A. Roos, Copper oxides [Cu 2 O, CuO], Handbook of Optical Constants of Solids, Elsevier, 1997, pp. 875–882.
[23] M.E. Sánchez-Vergara, et al., Determination of the optical GAP in thin films of amorphous dilithium phthalocyanine using the Tauc and Cody models, Molecules 17 (9) (2012) 10000–10013.
[24] Y. Bendale, V. Bendale, S. Paul, Evaluation of cytotoxic activity of platinum nanoparticles against normal and cancer cells and its anticancer potential through induction of apoptosis, Integr. Med. Res. 6 (2) (2017) 141–148.
[25] P. Pourali, S.H. Badiee, S. Manafi, T. Noorani, A. Rezaei, B. Yahyaei, Biosynthesis of gold nanoparticles by two bacterial and fungal strains, *Bacillus cereus* and *Fusarium oxysporum*, and assessment and comparison of their nanotoxicity in vitro by direct and indirect assays, Electron. J. Biotechnol. 29 (2017) 86–93.
[26] T. Muthukumar, B. Sambandam, A. Aravinthan, T.P. Sastry, J.H. Kim, Green synthesis of gold nanoparticles and their enhanced synergistic antitumor activity using HepG2 and MCF7 cells and its antibacterial effects, Process. Biochem. 51 (3) (2016) 384–391.
[27] S. Ghosh, A.N. Harke, M.J. Chacko, S.P. Gurav, K.A. Joshi, A. Dhepe, K. Banerjee, Gloriosa superba mediated synthesis of silver and gold nanoparticles for anticancer applications, J. Nanomed. Nanotechnol. 7 (390) (2016) 2.
[28] R. Liu, Q. Pei, T. Shou, W. Zhang, J. Hu, W. Li, Apoptotic effect of green synthesized gold nanoparticles from Curcuma wenyujin extract against human renal cell carcinoma A498 cells, Int. J. Nanomed. 14 (2019) 4091.
[29] D. Tang, Y. Dong, H. Ren, L. Li, C. He, A review of phytochemistry, metabolite changes, and medicinal uses of the common food mung bean and its sprouts [Vigna radiata], Chem. Cent. J. 8 (1) (2014) 4.
[30] N.P. Krishnappa, S.A. Basha, P.S. Negi, U.J. Prasada Rao, Phenolic acid composition, antioxidant and antimicrobial activities of green gram [vigna radiata] exudate, husk, and germinated seed of different stages, J. Food Process. Preserv. 41 (6) (2017)e13273.
[31] F. Wu, J. Zhu, G. Li, J. Wang, V.P. Veeraraghavan, S. Krishna Mohan, Q. Zhang, Biologically synthesized green gold nanoparticles from Siberian ginseng induce growth-inhibitory effect on melanoma cells [B16], Artif. Cells Nanomed. Biotechnol. 47 (1) (2019) 3297–3305.
[32] M. Nagalingam, V.N. Kalpana, A. Panneerselvam, Biosynthesis, characterization, and evaluation of bioactivities of leaf extract-mediated biocompatible gold nanoparticles from Alternanthera bettzickiana, Biotechnol. Rep. 19 (2018)e00268.
[33] A.A. Kajani, A.K. Bordbar, S.H.Z. Esfahani, A. Razmjou, Gold nanoparticles as potent anticancer agent: green synthesis, characterization, and in vitro study, RSC Adv. 6 (68) (2016) 63973–63983.
[34] A. Schröfel, G. Kratošová, Biosynthesis of metallic nanoparticles and their applications, in: A. Prokop (Ed.), Intracellular Delivery: Fundamentals and Applications, Springer Netherlands, Dordrecht, 2011, pp. 373–409, doi:http://dx.doi.org/10.1007/978-94-007-1248-5_14.
[35] P. Balashanmugam, P. Durai, M.D. Balakumaran, P.T. Kalaichelvan, Phytosynthesized gold nanoparticles from C. roxburghii DC. leaf and their toxic effects on normal and cancer cell lines, J. Photochem. Photobiol. B, Biol. 165 (2016) 163–173.
[36] S.K. Kamal, J. Vimala, P.K. Sahoo, P. Ghosal, S. Ram, L. Durai, A green chemical approach for synthesis of shape anisotropic gold nanoparticles, Int. Nano Lett. 4 (2) (2014) 109.
[37] A.I. Lukman, B. Gong, C.E. Marjo, U. Roessner, A.T. Harris, Facile synthesis, stabilization, and anti-bacterial performance of discrete Ag nanoparticles using Medicago sativa seed exudates, J. Colloid Interface Sci. 353 (2) (2011) 433–444.
[38] A.B.D. Nandiyanto, R. Oktiani, R. Ragadhita, How to read and interpret FTIR spectroscope of organic material, Indones. J. Sci. Technol. 4 (1) (2019) 97–118.
[39] K. Anand, R.M. Gengan, A. Phulukdaree, A. Chuturgoon, Agroforestry waste Moringa oleifera petals mediated green synthesis of gold nanoparticles and their anti-cancer and catalytic activity, J. Ind. Eng. Chem. 21 (2015) 1105–1111.
[40] V. Sunderam, D. Thiyagarajan, A.V. Lawrence, S.S.S. Mohammed, A. Selvaraj, In-vitro antimicrobial and anticancer properties of green synthesized gold nanoparticles using Anacardium occidentale leaves extract, Saudi J. Biol. Sci. 26 (3) (2019) 455–459.
[41] R. Geetha, T. Ashokkumar, S. Tamilselvan, K. Govindaraju, M. Sadiq, G. Singaravelu, Green synthesis of gold nanoparticles and their anticancer activity, Cancer Nanotechnol. 4 (4–5) (2013) 91–98.
[42] E.S. Al-Sheddi, N.N. Farshori, M.M. Al-Oqail, S.M. Al-Massarani, Q. Saquib, R. Wahab, M.A. Siddiqui, Anticancer potential of green synthesized silver nanoparticles using extract of Nepeta deflersiana against human cervical cancer cells [HeLA], Bioinorg. Chem. Appl. 2018 (2018).
[43] S. Nindawat, V. Agrawal, Fabrication of silver nanoparticles using Arnebia hispidissima [Lehm.] A. DC. Root extract and unravelling their potential biomedical applications, Artif. Cells Nanomed. Biotechnol. 47 (1) (2019) 166–180.
[44] C.Y. Looi, A. Arya, F.K. Cheah, B. Muharram, K.H. Leong, K. Mohamad, M.R. Mustafa, Induction of apoptosis in human breast cancer cells via caspase pathway by vernodalin isolated from Centratherum anthelminticum [L.] seeds, PLoS One 8 (2) (2013).
[45] Y. Yang, X. Du, Q. Wang, J. Liu, E. Zhang, L. Sai, H. Shao, Mechanism of cell death induced by silica nanoparticles in hepatocyte cells is by apoptosis, Int. J. Mol. Med. 44 (3) (2019) 903–912.
[46] A.A. Al-kawmani, K.M. Alanazi, M.A. Farah, M.A. Ali, W.A.Q. Hailan, F.M. Al-Hemaid, Apoptosis-inducing potential of biosynthesized silver nanoparticles in breast cancer cells, J. King Saud Univ. Sci. (2020).
[47] B.P.A. George, N. Kumar, H. Abrahamse, S.S. Ray, Apoptotic efficacy of multifaceted biosynthesized silver nanoparticles on human adenocarcinoma cells, Sci. Rep. 8 (1) (2018) 1–14.
[49] T. Zhang, L. Ma, P. Wu, W. Li, T. Li, R. Gu, Z. Xiao, Gallic acid has anticancer activity and enhances the anticancer effects of cisplatin in non-small cell lung cancer A549 cells via the JAK/STAT3 signaling pathway, Oncol. Rep. 41 (3) (2019) 1779-178.